

---

# How to build a consistency model: Learning flow maps via self-distillation

---

Nicholas M. Boffi  
Carnegie Mellon University

Michael S. Albergo  
Harvard University

Eric Vanden-Eijnden  
Courant Institute of Mathematical Sciences

## Abstract

Building on the framework proposed in [Boffi et al. \(2024\)](#), we present a systematic approach for learning flow maps associated with flow and diffusion models. Flow map-based models, commonly known as consistency models, encompass recent efforts to improve the efficiency of generative models based on solutions to differential equations. By exploiting a relationship between the velocity field underlying a continuous-time flow and the instantaneous rate of change of the flow map, we show how to convert existing distillation schemes into direct training algorithms via self-distillation, eliminating the need for pre-trained models. We empirically evaluate several instantiations of our framework, finding that high-dimensional tasks like image synthesis benefit from objective functions that avoid temporal and spatial derivatives of the flow map, while lower-dimensional tasks can benefit from objectives incorporating higher-order derivatives to capture sharp features.

## 1 Introduction

Generative models based on dynamical systems, such as flows and diffusions, have recently witnessed tremendous success in vision and language ([Song et al., 2020](#); [Rombach et al., 2022](#); [Ma et al., 2024](#); [Polyak et al., 2025](#)), as well as in scientific domains such as protein structure prediction ([Abramson et al., 2024](#)) and materials creation ([Zeni et al., 2025](#)). While highly expressive, these techniques require the solution of a differential equation for sample generation, which typically necessitates evaluation of the learned model tens to hundreds of times. As a result, their utility has been limited in domains where rapid inference is crucial, such as interactive decision-making, real-time control ([Black et al., 2024](#); [Chi et al., 2024](#)), and image editing, which has generated intense interest in acceleration of the underlying sampling procedure used for inference.

One promising approach, which underlies consistency models and their extensions ([Song et al., 2023](#); [Kim et al., 2024](#)), is to estimate the *flow map* associated with the solution of a differential equation instead of the vector field governing the instantaneous dynamics. The flow map corresponds to the integrated velocity field, and can therefore be used to directly generate samples in as few as one step. Recently, there has been broad effort to learn the flow map either directly or by distillation of a pre-trained model ([Boffi et al., 2024](#); [Frans et al., 2024](#); [Zhou et al., 2025](#); [Salimans et al., 2024](#)). Distillation-based approaches empirically perform well, but they require a two-phase learning setup, and the performance of the student is ultimately limited by the performance of the teacher. Ideally, the flow map could be trained directly without resorting to such an approach.

A fundamental challenge hindering direct training is the lack of an explicit characterization of the flow map that can be used to devise efficient training schemes, leading to complex pipelines that require extensive engineering to overcome unstable optimization dynamics. Here, building on the results

from Boffi et al. (2024), we propose a unifying framework that pairs the simplicity of flow-based training with the efficiency and efficacy of distillation. In typical distillation schemes, we first learn a score (Song and Ermon, 2020; Ho et al., 2020) or flow matching (Lipman et al., 2022; Albergo and Vanden-Eijnden, 2022; Albergo et al., 2023; Liu et al., 2022) model to estimate the underlying velocity. This network is then converted into a flow map via a secondary training algorithm that considers the pre-trained model as a “teacher” for the “student” flow map model. By leveraging three equivalent characterizations of the flow map, we show how many existing distillation schemes can be seen as minimizing the residual of a particular characterization. Making use of a simple tangent condition that relates the velocity of the flow to the derivative of the flow map, we show how any such scheme can be converted into a single, continual learning paradigm for the map alone. The result is a simple pipeline that can leverage off-the-shelf training procedures for flow- and score-based models to learn an accelerated sampler. Overall:

*We introduce a framework for self-distillation, showing how any distillation method for a consistency model can be converted into a direct training scheme.*

In particular, our main contributions are:

1. **Unifying perspective.** We provide a formal description of the flow map, which we show immediately leads to various recent few-step generative modeling algorithms such as consistency models and their extensions.
2. **Algorithms.** Leveraging our description of the flow map, we introduce three algorithms – Eulerian (ESD), Lagrangian (LSD), and Progressive Self-Distillation (PSD) – and discuss their connections to existing direct training schemes. We prove that each has the correct unique minimizer, and provide guarantees that the loss values bound the 2-Wasserstein error of the learned one-step model for ESD and LSD.
3. **Comparative Experiments.** We study the performance of each method as a function of the number of spatial and time derivatives that appear in the objective function. We show that with network architectures commonly used for flow models such as the U-Net, avoiding higher-order derivatives leads to systematically improved performance for image synthesis due to a reduction in gradient variance, while few-step performance can be better on low-dimensional datasets that require the representation of sharp features.

## 1.1 Related work

**Flow matching and diffusion models.** Our methods directly build on results from flow matching and stochastic interpolant methods (Lipman et al., 2022; Albergo and Vanden-Eijnden, 2022; Albergo et al., 2023; Liu et al., 2022) as well as the probability flow equation associated with diffusion models (Song et al., 2020; Ho et al., 2020; Maoutsa et al., 2020; Boffi and Vanden-Eijnden, 2023). These methods define an ordinary differential equation (ODE) whose solution provides the evaluation of the flow map at a specified time, while we seek to directly learn the two-time flow map itself. Our proposed approach exploits a condition that relates the flow map to the velocity field governing such probability flows. Due to the computational expense associated with solving these equations, a line of recent work asks how to resolve the flow more efficiently with higher-order numerical solvers (Dockhorn et al., 2022; Lu et al., 2022; Karras et al., 2022a; Li et al., 2024) and parallel sampling schemes (Chen et al., 2024; Bortoli et al., 2025). We take a different approach, opting to estimate an object that directly leads to accelerated sampling.

**Consistency models and distillation.** Appearing under several names, the flow map has become a central object of study in recent efforts to obtain accelerated sampling algorithms. Consistency models (Song et al., 2023; Song and Dhariwal, 2023) estimate the single-time flow map, which jumps directly from noise to data. Consistency trajectory models (Kim et al., 2024) and their generalizations (Li and He, 2025; Luo et al., 2023) estimate the two-time flow map, leading to multistep sampling. Both of these methods use an “Eulerian” characterization of the flow map, which we study and find leads to gradient instability. Progressive distillation (Salimans and Ho, 2022a) aims to obtain a model that can replicate two steps of the teacher; as we discuss below, this leverages a “semigroup” characterization of the flow map in terms of its composition. Related to our approach, shortcut models (Frans et al., 2024) introduce an algorithmic heuristic based on self-distillation, which our framework shows is a way to enforce the semigroup condition. This paper extends the flow map

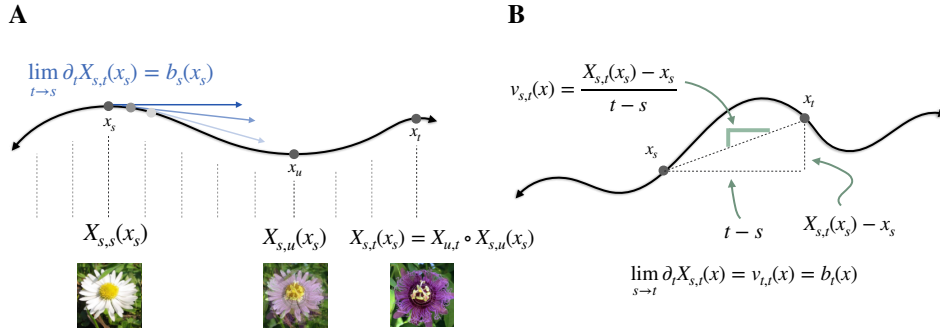


**Figure 1: Overview.** (A) Schematic of the two-time flow map  $X_{s,t}$  and the tangent condition (Lemma 2.1), which provides a relation between the map and the drift of the probability flow. The flow map is composable, invertible, and has the property that as  $t \rightarrow s$ , its time derivative recovers the drift  $b_s$  from (2). (B) Illustration of our proposed parameterization. The function  $v_{s,t}$  estimates the slope of the line drawn between two points on a trajectory of the probability flow, and can be directly trained efficiently via the tangent condition.

matching framework (Boffi et al., 2024) by studying all three map characterizations, demonstrating their use in distillation schemes with pre-trained velocity fields, and relating them to existing methods. We also show how these characterizations can be repurposed for *self-distillation*, i.e. direct training of the flow map.

## 2 Theoretical framework

In this work, we study the *flow map* of the probability flow equation, which is a function that jumps between points along a trajectory. Given access to the flow map, samples can be generated in a single step by jumping directly to the endpoint, or can be generated with an adaptively-determined amount of computation at inference time by taking multiple steps. In the following, we give a detailed mathematical description of the flow map, which we leverage to design a suite of novel direct training schemes. We begin with a review of the stochastic interpolant framework, which we leverage to build efficient and flexible generative models.

### 2.1 Stochastic interpolants and probability flows

Let  $\mathcal{D} = \{x_1^i\}_{i=1}^n$  with each  $x_1^i \in \mathbb{R}^d$ ,  $x_1^i \sim \rho_1$  denote a dataset drawn from a target density  $\rho_1$ . Given  $\mathcal{D}$ , our goal is to draw a fresh sample  $\hat{x}_1 \sim \hat{\rho}_1$  from a distribution  $\hat{\rho}_1 \approx \rho_1$  learned to approximate the target. Recent state of the art methods for accomplishing this task leverage flow-based representations, which dynamically evolve samples from a simple base distribution such as a standard Gaussian until they resemble samples from  $\rho_1$ .

**Interpolants.** To build a flow-based generative model, we leverage the stochastic interpolant framework, which we now briefly recall. For further details, the reader is referred to Albergo et al. (2023). We define a *stochastic interpolant* as a stochastic process  $I : [0, 1] \times \mathbb{R}^d \times \mathbb{R}^d \rightarrow \mathbb{R}^d$  that linearly combines samples from the target and the base,

$$I_t(x_0, x_1) = \alpha_t x_0 + \beta_t x_1, \quad (1)$$

where  $\alpha, \beta : [0, 1] \rightarrow [0, 1]$  are continuously differentiable functions satisfying the boundary conditions  $\alpha_0 = 1, \alpha_1 = 0, \beta_0 = 0$ , and  $\beta_1 = 1$ . In (1), the pair  $(x_0, x_1) \sim \rho(x_0, x_1)$  is drawn from a coupling satisfying the marginal constraints  $\int_{\mathbb{R}^d} \rho(x_0, x_1) dx_0 = \rho_1(x_1)$  and  $\int_{\mathbb{R}^d} \rho(x_0, x_1) dx_1 = \rho_0(x_0)$ . By construction, the probability density  $\rho_t = \text{Law}(I_t)$  defines a path in the space of measures between the base and the target. This path specifies a probability flow that pushes samples from  $\rho_0$  onto  $\rho_1$ ,

$$\dot{x}_t = b_t(x_t), \quad x_{t=0} = x_0 \sim \rho_0, \quad (2)$$

which has the same distribution as the interpolant,  $x_t \sim \rho_t$  for all  $t \in [0, 1]$ . The drift  $b$  in (2) is given by the conditional expectation of the time derivative of the interpolant,  $b_t(x) = \mathbb{E}[\dot{I}_t | I_t = x]$ , which averages the “velocity” of all interpolant paths that cross the point  $x$  at time  $t$ . A standard choice of coefficients is  $\alpha_t = 1 - t$  and  $\beta_t = t$  (Albergo and Vanden-Eijnden, 2022; Albergo et al., 2023), which recovers flow matching (Lipman et al., 2022) and rectified flow (Liu et al., 2022). Many other options have been considered in the literature, and in addition to flow matching, variance-preserving and variance-exploding diffusions can be obtained as particular cases.

**Learning.** By standard results in probability theory, the conditional expectation  $b_t$  can be learned efficiently in practice by solving a square loss regression problem,

$$b = \underset{\hat{b}}{\operatorname{argmin}} \mathcal{L}_b(\hat{b}), \quad \mathcal{L}_b(\hat{b}) = \int_0^1 \mathbb{E}_{x_0, x_1} [|\hat{b}_t(I_t) - \dot{I}_t|^2] dt. \quad (3)$$

Above,  $\mathbb{E}_{x_0, x_1}$  denotes an expectation over the random draws of  $(x_0, x_1)$  in the interpolant (1).

**Sampling.** Given an estimate  $\hat{b}$  obtained by minimizing (3) over a class of neural networks, we can generate an approximate sample  $\hat{x}_1$  by numerically integrating the learned probability flow  $\dot{\hat{x}}_t = \hat{b}_t(\hat{x}_t)$  until time  $t = 1$  from an initial condition  $\hat{x}_{t=0} \sim \rho_0$ . This approach yields high-quality samples from complex data distributions in practice, but is computationally expensive due to the need to repeatedly evaluate the learned model during integration.

## 2.2 Characterizing the flow map

The *flow map*  $X : [0, 1]^2 \times \mathbb{R}^d \rightarrow \mathbb{R}^d$  is the unique map satisfying the jump condition

$$X_{s,t}(x_s) = x_t \text{ for all } (s, t) \in [0, 1]^2, \quad (4)$$

where  $(x_t)_{t \in [0, 1]}$  is any solution of (2). The condition (4) means that the flow map takes “steps” of arbitrary size  $t - s$  along trajectories of the probability flow. In particular, a single application  $X_{0,1}(x_0)$  with  $x_0 \sim \rho_0$  yields a sample from  $\rho_1$ , avoiding numerical integration entirely.

In what follows, we give three characterizations of the flow map that each lead to an objective for its estimation. As we now show, these characterizations are based on a simple but key result that shows we can deduce the corresponding velocity field  $b_t$  from a given flow map  $X_{s,t}$ .

**Lemma 2.1** (Tangent condition). *Let  $X_{s,t}$  denote the flow map. Then,*

$$\lim_{s \rightarrow t} \partial_t X_{s,t}(x) = b_t(x) \quad \forall t \in [0, 1], \quad \forall x \in \mathbb{R}^d, \quad (5)$$

*i.e. the tangent vectors to the curve  $(X_{s,t}(x))_{t \in [s, 1]}$  give the velocity field  $b_t(x)$  for every  $x$ .*

As illustrated in Figure 1A, Lemma 2.1 highlights that there is a velocity model “implicit” in a flow map. To leverage this algorithmically, we propose to adopt an Euler step-like parameterization that takes into account the boundary condition  $X_{s,s}(x) = x$ ,

$$X_{s,t}(x) = x + (t - s)v_{s,t}(x). \quad (6)$$

In (6),  $v : [0, 1]^2 \times \mathbb{R}^d \rightarrow \mathbb{R}^d$  is the function we will estimate over neural networks. Mathematically,  $v_{s,t}$  can be interpreted as the exact remainder obtained by truncating a Taylor expansion in  $t - s$  of  $X_{s,t}(x)$  at first order. Since (6) implies that  $\lim_{s \rightarrow t} \partial_t X_{s,t}(x) = v_{t,t}(x)$ , we obtain:

$$v_{t,t}(x) = b_t(x), \quad \forall t \in [0, 1], \quad \forall x \in \mathbb{R}^d. \quad (7)$$

Geometrically,  $v_{s,t}$  describes the “slope” of the line drawn between  $x_s$  and  $x_t$  on a single ODE trajectory (Figure 1B). The condition (7) states that the slope between two infinitesimally-spaced points is precisely the velocity  $b_t$ . A key realization is that this indicates  $v_{t,t}$  can be estimated using the objective (3). To learn the map  $X_{s,t}$ , it then remains to estimate  $v_{s,t}$  away from the diagonal  $s = t$  of the unit square. To this end, we leverage the following result.

**Proposition 2.2** (Flow map). *Assume that  $X_{s,t}$  is given by (6) with  $v_{s,t}$  satisfying (7). Then,  $X_{s,t}$  is the flow map defined in (4) if any of the following conditions also holds:*

(i) (Lagrangian condition):  $X_{s,t}$  solves the Lagrangian equation

$$\partial_t X_{s,t}(x) = v_{t,t}(X_{s,t}(x)), \quad (8)$$

*for all  $(s, t) \in [0, 1]^2$  and for all  $x \in \mathbb{R}^d$ .*

(ii) (Eulerian condition):  $X_{s,t}$  solves the Eulerian equation

$$\partial_s X_{s,t}(x) + \nabla X_{s,t}(x) v_{s,s}(x) = 0, \quad (9)$$

*for all  $(s, t) \in [0, 1]^2$  and for all  $x \in \mathbb{R}^d$ .*



- (iii) (Semigroup condition): For all  $(s, t, u) \in [0, 1]^3$  and for all  $x \in \mathbb{R}^d$ ,
- $$X_{u,t}(X_{s,u}(x)) = X_{s,t}(x). \quad (10)$$

The Lagrangian and Eulerian conditions in Proposition 2.2 categorize the flow map  $X_{s,t}$  as the solution of an infinite system of ODEs or as the solution of a PDE, each of which describes transport along trajectories of the flow (2). The semigroup condition states that any two jumps can be replaced by a single jump. Appendix B provides a brief review of the flow map matching framework, which shows how these three characterizations are the basis for consistency and progressive distillation schemes that have appeared in the literature. In the following, we show how each – and in fact how *any* distillation method that produces a flow map from a velocity field  $\hat{b}$  – can be immediately converted into a *direct training* objective for a single network model  $X_{s,t}$  via the concept of self-distillation.

### 2.3 A framework for self-distillation

Our framework augments training of  $v_{t,t}$  via the objective (3) and the identity (7) on the diagonal  $s = t$  with a penalization term for at least one of the conditions in Proposition 2.2 along the off-diagonal  $s < t$ . This leads to a series of objectives that can be used to learn the map.

**Proposition 2.3** (Self-distillation). *The flow map  $X_{s,t}$  defined in (4) is given for all  $0 \leq s \leq t \leq 1$  by  $X_{s,t}(x) = x + (t - s)v_{s,t}(x)$  where  $v_{s,t}(x)$  the unique minimizer over  $\hat{v}$  of*

$$\mathcal{L}_{\text{SD}}(\hat{v}) = \mathcal{L}_b(\hat{v}) + \mathcal{L}_{\text{D}}(\hat{v}), \quad (11)$$

where  $\mathcal{L}_b(\hat{v})$  is given by

$$\mathcal{L}_b(\hat{v}) = \int_0^1 \mathbb{E}_{x_0, x_1} [|\hat{v}_{t,t}(I_t) - \dot{I}_t|^2] dt, \quad (12)$$

and where  $\mathcal{L}_{\text{D}}(\hat{v})$  is any linear combination of the following three objectives.

- (i) The Lagrangian self-distillation (LSD) objective, which leverages (8),

$$\mathcal{L}_{\text{D}}^{\text{LSD}}(\hat{v}) = \int_0^1 \int_0^t \mathbb{E}_{x_0, x_1} [|\partial_t \hat{X}_{s,t}(I_s) - \hat{v}_{t,t}(\hat{X}_{s,t}(I_s))|^2] ds dt; \quad (13)$$

- (ii) The Eulerian self-distillation (ESD) objective, which leverages (9),

$$\mathcal{L}_{\text{D}}^{\text{ESD}}(\hat{v}) = \int_0^1 \int_0^t \mathbb{E}_{x_0, x_1} [|\partial_s \hat{X}_{s,t}(I_s) + \nabla \hat{X}_{s,t}(I_s) \hat{v}_{t,t}(I_s)|^2] ds dt; \quad (14)$$

- (iii) The progressive self-distillation (PSD) objective, which leverages (10),

$$\mathcal{L}_{\text{D}}^{\text{PSD}}(\hat{v}) = \int_0^1 \int_0^t \int_s^t \mathbb{E}_{x_0, x_1} [|\hat{X}_{s,t}(I_s) - \hat{X}_{u,t}(\hat{X}_{s,u}(I_s))|^2] du ds dt. \quad (15)$$

Above,  $\hat{X}_{s,t}(x) = x + (t - s)\hat{v}_{s,t}(x)$  and  $\mathbb{E}_{x_0, x_1}$  denotes an expectation over the random draws of  $(x_0, x_1)$  in the interpolant defined in (1).

The proof follows directly from Proposition 2.2 and is given in Appendix C; the resulting algorithmic approach is summarized graphically in Figure 2. In Proposition 2.3, we focus on  $s \leq t$ , which is all that is required to generate data. Training over the entire unit square  $(s, t) \in [0, 1]^2$  also enables jumping from data to noise along trajectories of (2). The derivatives with respect to space and time required to implement the LSD and ESD losses can be computed efficiently via standard jvp implementations available in jax and pytorch. As we will see in the experiments, an advantage of the scheme (15) is that it avoids derivatives with respect to time and space, which leads to improved training stability. We now provide theoretical guarantees that the objective value bounds the accuracy of the model for both LSD and ESD. We were unable to obtain a similar guarantee for PSD, which we leave to future work.

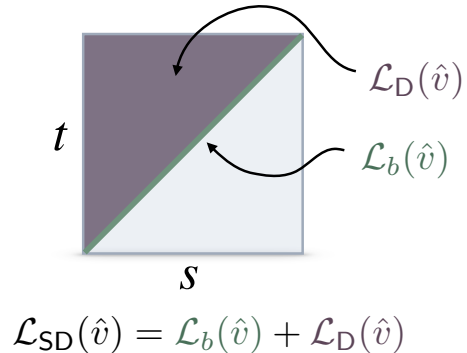


**Figure 2: Self-distillation.** Our plug-and-play approach pairs any distillation objective  $\mathcal{L}_{\text{D}}$  on the off-diagonal  $s < t$  of the square  $[0, 1]^2$  with a flow matching objective  $\mathcal{L}_b$  on the diagonal  $s = t$  to obtain a direct training algorithm for the flow map.

---

**Algorithm 1:** Learning flow maps via self-distillation

---

**input:** Samples from  $\rho(x_0, x_1)$ ; coefficients  $\alpha_t, \beta_t$ ; batch size  $M$ ; time sampling distribution  $p_{st}$ ; distillation objective  $\mathcal{L}_D$ .

**repeat**

    Draw batch  $(s_i, t_i, x_0^i, x_1^i)_{i=1}^M \sim p \times \rho$ .

    Compute  $I_{s_i} = \alpha_{s_i} x_0^i + \beta_{s_i} x_1^i$ ,  $I_{t_i} = \alpha_{t_i} x_0^i + \beta_{t_i} x_1^i$ ,  $\dot{I}_{t_i} = \dot{\alpha}_{t_i} x_0^i + \dot{\beta}_{t_i} x_1^i$ .

    Compute  $\hat{\mathcal{L}}_{SD}(\hat{v}) = \frac{1}{n} \sum_{i=1}^n (|\hat{v}_{t_i}(I_{t_i}) - \dot{I}_{t_i}|^2 + \mathcal{L}_D^{s_i, t_i}(\hat{v}))$ .

    Take gradient step on  $\hat{\mathcal{L}}_{SD}$  to update  $\hat{v}$ .

**until** converged;

**output:** Flow map  $\hat{X}$

---

**Proposition 2.4** (Wasserstein bounds). *Let  $\hat{X}_{s,t}(x) = x + (t-s)\hat{v}_{s,t}(x)$  denote a candidate flow map satisfying  $\mathcal{L}_b(\hat{v}) + \mathcal{L}_D^{ESD}(\hat{v}) \leq \varepsilon$ , and let  $\hat{\rho}_1$  denote the corresponding pushforward  $\hat{\rho}_1 = \hat{X}_{0,1\#}\rho_0$ . Let  $\hat{L}$  denote the spatial Lipschitz constant of  $\hat{v}_{t,t}(\cdot)$ . Then,*

$$W_2^2(\hat{\rho}_1, \rho_1) \leq 4e^{1+2\hat{L}}\varepsilon. \quad (16)$$

Now assume that  $\mathcal{L}_b(\hat{v}) + \mathcal{L}_D^{ESD}(\hat{v}) \leq \varepsilon$ . Then,

$$W_2^2(\hat{\rho}_1, \rho_1) \leq 2e(1 + e^{2\hat{L}})\varepsilon. \quad (17)$$

The above result highlights that the model’s accuracy improves systematically as the loss is minimized for both ESD and LSD. The proof follows by combining guarantees for distillation-based algorithms with guarantees for flow-based algorithms. The assumptions imply that the model  $\hat{v}_{t,t}$  is an accurate flow and that  $\hat{X}_{s,t}$  has accurately distilled it, enabling us to stitch together two classes of guarantees.

### 3 Algorithmic aspects

We now provide practical numerical recommendations for an effective implementation of self-distillation. Our aim is not to provide a single best-choice method, but to devise a general-purpose framework that can be used to build high-performing consistency models across data modalities. We anticipate the best scheme to be problem, dataset, and architecture-dependent.

**Multiple models.** In Proposition 2.3, we emphasize the use of a single model  $\hat{X}_{s,t}$  defined in terms of the function  $\hat{v}_{s,t}$ . While this approach leads to greater efficiency, it requires the model to learn strictly more than the velocity field  $\hat{b}$  typically learned in traditional flow-based methods. If the computational budget is available, our framework may also be used with two separate models – one parameterizing the flow  $\hat{b}$ , and one parameterizing the map  $\hat{X}_{s,t}$  – which can be trained simultaneously. Moreover, alternative parameterizations may be designed that leverage these multiple models directly; for example, with the second order Taylor expansion-like representation

$$\hat{X}_{s,t}(x) = x + (t-s)b_t(x) + \frac{1}{2}(t-s)^2\psi_{s,t}(x), \quad (18)$$

we may leverage a pre-trained model  $\hat{b}_t$  directly in the representation of  $\hat{X}$ , or parameterize it with a second network that may be trained in tandem with  $\psi$ .

**General representations.** While the parameterization (6) leads to a simple learning scheme for  $\hat{v}$ , any parameterization  $\hat{X}_{s,t}$  satisfying  $\hat{X}_{s,s}(x) = x$  for all  $s \in [0, 1]$  and for all  $x \in \mathbb{R}^d$  may be used in practice. In this more general case, we may replace every appearance of  $\hat{v}_{t,t}$  by  $\lim_{s \rightarrow t} \partial_t \hat{X}_{s,t}(x) = \partial_t \hat{X}_{s,t}(x)|_{s=t}$ , which can be computed via automatic differentiation. In the experiments, we focus on (6) for simplicity and computational efficiency.

**Loss weighting.** The loss (11) can be written explicitly as an integral over the upper triangle  $s < t$ ,

$$\mathcal{L}_{SD}(\hat{v}) = \int_0^1 \int_0^t (\mathcal{L}_b^t(\hat{v})\delta(s-t) + \mathcal{L}_D^{s,t}(\hat{v})) ds dt, \quad (19)$$

where  $\mathcal{L}_b^t(\hat{v}) = \mathbb{E}_{x_0, x_1} [|\hat{v}_{t,t}(I_t) - \dot{I}_t|^2]$  denotes the interpolant loss restricted to  $t$ , and where  $\mathcal{L}_D^{s,t}(\hat{v})$  similarly denotes the distillation term restricted to the pair  $(s, t)$ . In practice, we find that loss values at different pairs  $(s, t)$  can have gradient norms that differ significantly, introducing variance into the loss estimate. To rectify this, we incorporate a learned weighting function  $w_{s,t}$  similar to EDM2 (Karras et al., 2024),

$$\mathcal{L}_{SD}(\hat{v}) = \int_0^1 \int_0^t (e^{-w_{s,t}} (\mathcal{L}_b^t(\hat{v})\delta(s-t) + \mathcal{L}_D^{s,t}(\hat{v})) + w_{s,t}) ds dt. \quad (20)$$

In (20),  $w_{s,t}$  can be interpreted as an estimate of the log-variance of the loss values; at the global minimizer, it ensures that all values of  $(s, t)$  contribute on a similar scale. We find that the use of  $w_{s,t}$  significantly stabilizes the training dynamics and enables the use of larger learning rates.

**Temporal sampling.** Independent of the weight, we also introduce a sampling distribution  $p_{s,t}$ ,

$$\mathcal{L}_{SD}(\hat{v}) = \mathbb{E}_{p_{s,t}} [e^{-w_{s,t}} (\mathcal{L}_b^t(\hat{v})\delta(s-t) + \mathcal{L}_D^{s,t}(\hat{v})) + w_{s,t}]. \quad (21)$$

Let  $U_d$  denote a uniform distribution on the diagonal  $s = t$ , and let  $U_{od}$  denote a uniform distribution on the upper triangle  $s < t$ . In our experiments, we chose  $p = U_{od}$ . This induces a marginal distribution over  $t$  that is non-uniform,  $\int p_{st} dt = p_t \neq U_d$ , and which places quadratically more mass for  $t$  closer to 1. In early experiments, we found that this choice outperformed the mixture  $p_{s,t} = \eta U_d + (1 - \eta) U_{od}$  with a fraction  $\eta$  of samples uniformly distributed on the diagonal and a fraction  $(1 - \eta)$  uniformly distributed in the upper triangle for few-step sampling. Nevertheless, using a mixture distribution ensures that a proportion  $\eta$  of training is devoted to learning the probability flow from the external signal  $\dot{I}_t$ , while a fraction  $1 - \eta$  is devoted to distilling that external signal into a few-step map. The distillation objectives in Proposition 2.3 are more expensive than the interpolant objective, because they require multiple evaluations of the network and Jacobian-vector products. As a result,  $\eta$  can be used to tune the cost of each training step (Frans et al., 2024).

**PSD sampling.** For PSD, we introduce a proposal distribution  $p_u$  over the intermediate step,

$$\mathcal{L}_{SSD}^{s,t}(\hat{v}) = \mathbb{E}_{p_u} \mathbb{E}_{x_0, x_1} \left[ \left| \hat{X}_{s,t}(I_s) - \hat{X}_{u,t}(\hat{X}_{s,u}(I_s)) \right|^2 \right]. \quad (22)$$

We propose to parameterize  $u = \gamma s + (1 - \gamma)t$  as a convex combination for  $\gamma \in [0, 1]$ , and we define the proposal distribution by sampling over  $\gamma$ . In our numerical experiments, we compare uniform sampling (PSD-U) for  $\gamma \in [0, 1]$  to midpoint sampling where  $\gamma = 1/2$  deterministically (PSD-M), which corresponds to a continuous limit of shortcut models. Following Algorithm 1, SSD requires a batch of  $\gamma_i$  values to compute  $u_i = \gamma_i s_i + (1 - \gamma_i)t_i$ .

**PSD scaling.** We show in Appendix D that (22) may be rewritten as

$$\mathcal{L}_{SSD}^{s,t}(\hat{v}) = \mathbb{E}_{p_\gamma} \mathbb{E}_{x_0, x_1} \left[ \left| \hat{v}_{s,t}(I_s) - (1 - \gamma)\hat{v}_{s,u}(I_s) - \gamma\hat{v}_{u,t}(X_{s,u}(I_s)) \right|^2 \right]. \quad (23)$$

The representation (23) eliminates the factors  $u - s$ ,  $t - s$ , and  $t - u$  appearing in the  $\hat{X}$  evaluations due to the parameterization (6). We found that these terms introduced higher gradient variance because they cause the loss to scale like  $(t - s)^2$ , which changes the effective learning rate depending on the timestep  $t - s$ . By writing the loss in the form (23), we precondition the problem and remove this additional source of variability, which we found led to improved training stability.

**Annealing.** We show in Appendix D that both the Lagrangian (8) and Eulerian equation (9) reduce to the tangent condition (5) in the limit as  $s \rightarrow t$ . Moreover, we show that by taking  $u = t - h$  or  $u = s + h$  in the semigroup condition (10), we recover the Lagrangian and Eulerian equations in the limit as  $h \rightarrow 0$ . In this way, the off-diagonal self-distillation terms  $\mathcal{L}_D$  represent a natural extension of the diagonal flow matching term. This motivates a simple two-phase annealing strategy in which, to warm up the teacher, the flow matching term is trained alone for  $N_{fm}$  steps, followed by a smooth conversion from diagonal training into self-distillation by expanding the range of  $|t - s|$  for  $N_{anneal}$  steps. The teacher warmup may also be viewed as a pre-training phase, and can be skipped by initializing from a pre-trained velocity field model  $\hat{b}_t$  by duplicating the time embeddings. In practice, we found that this approach greatly accelerated and stabilized training. In our experiments, a simple linear expansion of  $|t - s|$  over  $N_{anneal} = 10,000$  steps worked well.

Method	Step Count				
	1	2	4	8	16
LSD	<b>0.0237</b>	0.0261	0.0275	0.0269	0.0258
ESD	0.0468	0.0414	0.0331	0.0243	0.0205
PSD-M	0.0772	0.0305	0.0212	0.0139	0.0115
PSD-U	0.0527	<b>0.0214</b>	<b>0.0167</b>	<b>0.0119</b>	<b>0.0085</b>

**Table 1: Checker dataset.** KL divergence ( $\downarrow$ ) as a function of the number of steps for sampling on the low-dimensional checker dataset. LSD performs best for single-step sampling, while PSD-U wins for more steps.

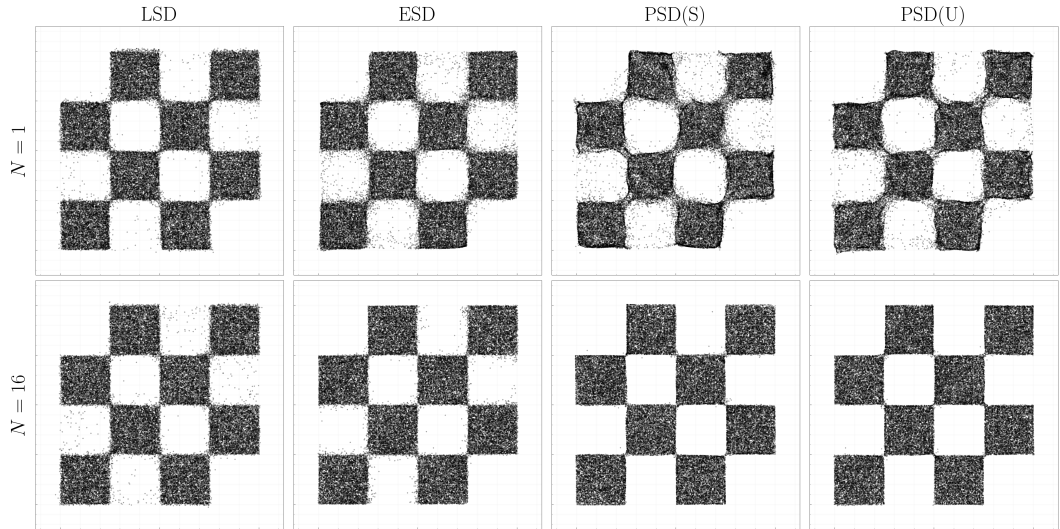


**Figure 3: Checker dataset.** Qualitative results for the two-dimensional checker dataset. For low numbers of sampling steps, the LSD and ESD methods introduce fewer boundary artifacts, while the PSD algorithms more effectively capture the sharp boundaries as the number of sampling steps increases.

**Choice of teacher.** The self-distillation objectives in Proposition 2.3 are written by squaring the residual of the properties in Proposition 2.2, but there are several options for defining the teacher via the use of the stopgrad operator  $\text{sg}(\cdot)$ . For LSD, we may “convexify” the objective by using  $\text{sg}(\hat{v}_{t,t}(\hat{X}_{s,t}(I_s)))$  as a teacher, which matches the distillation setting given a frozen pre-trained model. In addition to the placement of  $\text{sg}(\cdot)$ , we may either use the model  $\hat{v}_{t,t}$  with instantaneous parameters as the teacher, or we may use an exponential moving average (EMA). For networks that utilize dropout, we call the teacher network in evaluation mode to avoid additional variability.

## 4 Numerical results

We test LSD, ESD, and PSD on the low-dimensional checker dataset, which is less sensitive to specific network parameterization, and unconditional image generation on the CIFAR-10 dataset. For PSD, we consider two variants – PSD-U, which uses uniform sampling of  $\gamma$ , and PSD-M, which samples  $\gamma = 1/2$  deterministically and is related to shortcut models (Frans et al., 2024). Full training details are provided in Appendix E.

### 4.1 Low-dimensional generation

We first study model performance on the two-dimensional checker dataset. While low-dimensional, the checker exhibits multimodality and sharp cutoffs that make it a useful testbed for visualization of how few-step samplers capture complex features in the target. We use a four-layer MLP architecture with no time embedding, so that  $s$  and  $t$  are concatenated to the data point  $x$  as input to the network. Qualitative results are shown in Figure 3, while quantitative results obtained by estimating the KL

Method	Step Count				
	1	2	4	8	16
LSD	38.01	21.68	13.08	9.70	8.23
PSD-M	15.16	9.50	7.05	<b>5.75</b>	<b>5.13</b>
PSD-U	<b>14.13</b>	<b>8.59</b>	<b>7.04</b>	6.00	5.16

**Table 2: CIFAR-10.** FID ( $\downarrow$ ) as a function of the number of steps for unconditional image generation.



**Figure 5:** Progressive refinement using eight fixed noise samples for the three samplers.

divergence between generated samples and the target are shown in Table 1. The LSD algorithm performs best for a single sampling step, but does not improve significantly as the number of sampling steps increases. The ESD algorithm improves, but under-performs LSD for few sampling steps, and under-performs PSD for a larger number. The PSD algorithms struggle to capture the sharp features in few steps, but PSD-U produces the best results for two or more steps. Full qualitative visualization over the range shown in the table is depicted in Figure 6 (Appendix).

## 4.2 Unconditional image generation

We now consider unconditional image generation on the CIFAR-10 dataset. In Figure 4, we compare the (parameter) gradient norm as a function of the training iteration for LSD, PSD-U, PSD-M, and ESD. We find that PSD, which avoid computing temporal or spatial derivatives of the network during training, maintain significantly more stable gradients. Moreover, we found that the high gradient norms seen for ESD led to training instability that was difficult to control, ultimately leading to divergence. This is consistent with earlier work on consistency models, where careful annealing schedules, clipping, and network design has been used to reduce issues with gradient variance (Song and Dhariwal, 2023); here we show that these issues can be avoided by modifying the objective directly.

We track the quantitative performance of each method as measured by FID in Table 2, where we find that the gradient norm during training is predictive of model performance. We do not report FID values for the ESD method due to the observed training instability, which led to very low-quality images. We find that PSD-U obtains the best performance for low step count, while PSD-M obtains a slight edge for higher step count. A qualitative visualization of sample quality is shown in Figure 5 as a function of the number of sampling steps, where a fixed random seed is shown for comparison. We see that each method obtains systematically improved resolution as the number of steps increases, and that all methods produce similar images with an identical random seed. We emphasize that our goal here is not to attain state of the art performance, but to understand how each loss function affects training stability and sample quality; with further engineering, we anticipate that quantitative FID values could be lowered significantly for all methods. We leave a study of how alternative network architectures could be designed to improve the stability of LSD and ESD to future work.

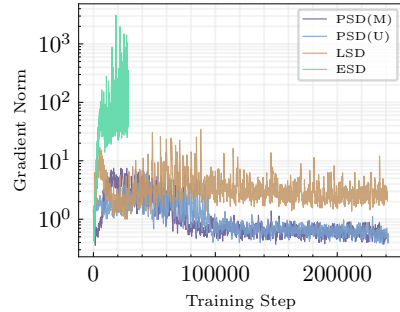


**Figure 4: Gradient norms vs SD method.** Spatial and time representations in the flow map impact gradient norms of SD methods that require derivatives w.r.t  $x$ ,  $s$ , or  $t$ .



## References

- Nicholas M. Boffi, Michael S. Albergo, and Eric Vanden-Eijnden. Flow Map Matching: A unifying framework for consistency models. *arXiv:2406.07507*, June 2024.
- Yang Song, Jascha Sohl-Dickstein, Diederik P Kingma, Abhishek Kumar, Stefano Ermon, and Ben Poole. Score-based generative modeling through stochastic differential equations. *arXiv:2011.13456*, 2020.
- Robin Rombach, Andreas Blattmann, Dominik Lorenz, Patrick Esser, and Björn Ommer. High-resolution image synthesis with latent diffusion models. In *Proceedings of the IEEE/CVF conference on computer vision and pattern recognition*, pages 10684–10695, 2022.
- Nanye Ma, Mark Goldstein, Michael S. Albergo, Nicholas M. Boffi, Eric Vanden-Eijnden, and Saining Xie. SiT: Exploring Flow and Diffusion-based Generative Models with Scalable Interpolant Transformers. *arXiv:2401.08740*, 2024.
- Adam Polyak, Amit Zohar, Andrew Brown, Andros Tjandra, Animesh Sinha, Ann Lee, Apoorv Vyas, Bowen Shi, Chih-Yao Ma, Ching-Yao Chuang, David Yan, Dhruv Choudhary, Dingkan Wang, Geet Sethi, Guan Pang, Haoyu Ma, Ishan Misra, Ji Hou, Jialiang Wang, Kiran Jagadeesh, Kunpeng Li, Luxin Zhang, Mannat Singh, Mary Williamson, Matt Le, Matthew Yu, Mitesh Kumar Singh, Peizhao Zhang, Peter Vajda, Quentin Duval, Rohit Girdhar, Roshan Sumbaly, Sai Saketh Rambhatla, Sam Tsai, Samaneh Azadi, Samyak Datta, Sanyuan Chen, Sean Bell, Sharadh Ramaswamy, Shelly Sheynin, Siddharth Bhattacharya, Simran Motwani, Tao Xu, Tianhe Li, Tingbo Hou, Wei-Ning Hsu, Xi Yin, Xiaoliang Dai, Yaniv Taigman, Yaqiao Luo, Yen-Cheng Liu, Yi-Chiao Wu, Yue Zhao, Yuval Kirstain, Zecheng He, Zijian He, Albert Pumarola, Ali Thabet, Arsiom Sanakoyeu, Arun Malloya, Baishan Guo, Boris Araya, Breena Kerr, Carleigh Wood, Ce Liu, Cen Peng, Dmitry Vengertsev, Edgar Schonfeld, Elliot Blanchard, Felix Juefei-Xu, Fraylie Nord, Jeff Liang, John Hoffman, Jonas Kohler, Kaolin Fire, Karthik Sivakumar, Lawrence Chen, Licheng Yu, Luya Gao, Markos Georgopoulos, Rashel Moritz, Sara K. Sampson, Shikai Li, Simone Parmeggiani, Steve Fine, Tara Fowler, Vladan Petrovic, and Yuming Du. Movie gen: A cast of media foundation models. *arXiv:2410.13720*, 2025.
- Josh Abramson, Jonas Adler, Jack Dunger, Richard Evans, Tim Green, Alexander Pritzel, Olaf Ronneberger, Lindsay Willmore, Andrew J. Ballard, Joshua Bambrick, Sebastian W. Bodenstein, David A. Evans, Chia-Chun Hung, Michael O’Neill, David Reiman, Kathryn Tunyasuvunakool, Zachary Wu, Akvilė Žemgulytė, Eirini Arvaniti, Charles Beattie, Ottavia Bertolli, Alex Bridgland, Alexey Cherepanov, Miles Congreve, Alexander I. Cowen-Rivers, Andrew Cowie, Michael Figurnov, Fabian B. Fuchs, Hannah Gladman, Rishub Jain, Yousuf A. Khan, Caroline M. R. Low, Kuba Perlin, Anna Potapenko, Pascal Savy, Sukhdeep Singh, Adrian Stecula, Ashok Thillaisundaram, Catherine Tong, Sergei Yakneen, Ellen D. Zhong, Michal Zielinski, Augustin Židek, Victor Bapst, Pushmeet Kohli, Max Jaderberg, Demis Hassabis, and John M. Jumper. Accurate structure prediction of biomolecular interactions with alphafold 3. *Nature*, 630(8016):493–500, 2024.
- Claudio Zeni, Robert Pinsler, Daniel Zügner, Andrew Fowler, Matthew Horton, Xiang Fu, Zilong Wang, Aliaksandra Shysheya, Jonathan Crabbé, Shoko Ueda, Roberto Sordillo, Lixin Sun, Jake Smith, Bichlien Nguyen, Hannes Schulz, Sarah Lewis, Chin-Wei Huang, Ziheng Lu, Yichi Zhou, Han Yang, Hongxia Hao, Jielan Li, Chunlei Yang, Wenjie Li, Ryota Tomioka, and Tian Xie. A generative model for inorganic materials design. *Nature*, 639(8055):624–632, 2025.
- Kevin Black, Noah Brown, Danny Driess, Adnan Esmail, Michael Equi, Chelsea Finn, Niccolo Fusai, Lachy Groom, Karol Hausman, Brian Ichter, Szymon Jakubczak, Tim Jones, Liyiming Ke, Sergey Levine, Adrian Li-Bell, Mohith Mothukuri, Suraj Nair, Karl Pertsch, Lucy Xiaoyang Shi, James Tanner, Quan Vuong, Anna Walling, Haohuan Wang, and Ury Zhilinsky.  $\pi_0$ : A Vision-Language-Action Flow Model for General Robot Control. *arXiv:2410.24164*, October 2024.
- Cheng Chi, Zhenjia Xu, Siyuan Feng, Eric Cousineau, Yilun Du, Benjamin Burchfiel, Russ Tedrake, and Shuran Song. Diffusion Policy: Visuomotor Policy Learning via Action Diffusion. *arXiv:2303.04137*, 2024.
- Yang Song, Prafulla Dhariwal, Mark Chen, and Ilya Sutskever. Consistency Models. *arXiv:2303.01469*, 2023.



- Dongjun Kim, Chieh-Hsin Lai, Wei-Hsiang Liao, Naoki Murata, Yuhta Takida, Toshimitsu Uesaka, Yutong He, Yuki Mitsufuji, and Stefano Ermon. Consistency Trajectory Models: Learning Probability Flow ODE Trajectory of Diffusion. *arXiv:2310.02279*, 2024.
- Kevin Frans, Danijar Hafner, Sergey Levine, and Pieter Abbeel. One step diffusion via shortcut models. *arXiv:2410.12557*, 2024.
- Linqi Zhou, Stefano Ermon, and Jiaming Song. Inductive moment matching. *arXiv:2503.07565*, 2025.
- Tim Salimans, Thomas Mensink, Jonathan Heek, and Emiel Hoogetboom. Multistep Distillation of Diffusion Models via Moment Matching. *arXiv:2406.04103*, June 2024.
- Yang Song and Stefano Ermon. Generative Modeling by Estimating Gradients of the Data Distribution. *arXiv:1907.05600*, 2020.
- Jonathan Ho, Ajay Jain, and Pieter Abbeel. Denoising diffusion probabilistic models. In *Advances in neural information processing systems*, volume 33, pages 6840–6851, 2020.
- Yaron Lipman, Ricky TQ Chen, Heli Ben-Hamu, Maximilian Nickel, and Matthew Le. Flow matching for generative modeling. In *The Eleventh International Conference on Learning Representations*, 2022.
- Michael S Albergo and Eric Vanden-Eijnden. Building normalizing flows with stochastic interpolants. In *The Eleventh International Conference on Learning Representations*, 2022.
- Michael S Albergo, Nicholas M Boffi, and Eric Vanden-Eijnden. Stochastic interpolants: A unifying framework for flows and diffusions. *arXiv preprint arXiv:2303.08797*, 2023.
- Xingchao Liu, Chengyue Gong, and Qiang Liu. Flow straight and fast: Learning to generate and transfer data with rectified flow. In *The Eleventh International Conference on Learning Representations*, 2022.
- Dimitra Maoutsa, Sebastian Reich, and Manfred Opper. Interacting particle solutions of Fokker-Planck equations through gradient-log-density estimation. *Entropy*, 22(8):802, July 2020.
- Nicholas M. Boffi and Eric Vanden-Eijnden. Probability flow solution of the Fokker–Planck equation. *Machine Learning: Science and Technology*, 4(3):035012, July 2023.
- Tim Dockhorn, Arash Vahdat, and Karsten Kreis. Genie: Higher-order denoising diffusion solvers. *arXiv:2210.05475*, 2022.
- Cheng Lu, Yuhao Zhou, Fan Bao, Jianfei Chen, Chongxuan Li, and Jun Zhu. Dpm-solver: A fast ode solver for diffusion probabilistic model sampling in around 10 steps. *arXiv:2206.00927*, 2022.
- Tero Karras, Miika Aittala, Timo Aila, and Samuli Laine. Elucidating the design space of diffusion-based generative models. *arXiv:2206.00364*, 2022a.
- Gen Li, Yu Huang, Timofey Efimov, Yuting Wei, Yuejie Chi, and Yuxin Chen. Accelerating convergence of score-based diffusion models, provably. *arXiv:2403.03852*, 2024.
- Haoxuan Chen, Yinuo Ren, Lexing Ying, and Grant M. Rotskoff. Accelerating diffusion models with parallel sampling: Inference at sub-linear time complexity. *arXiv:2405.15986*, 2024.
- Valentin De Bortoli, Alexandre Galashov, Arthur Gretton, and Arnaud Doucet. Accelerated diffusion models via speculative sampling. *arXiv:2501.05370*, 2025.
- Yang Song and Prafulla Dhariwal. Improved Techniques for Training Consistency Models. *arXiv:2310.14189*, 2023.
- Liangchen Li and Jiajun He. Bidirectional consistency models. *arXiv:2403.18035*, 2025.
- Simian Luo, Yiqin Tan, Longbo Huang, Jian Li, and Hang Zhao. Latent consistency models: Synthesizing high-resolution images with few-step inference. *arXiv:2310.04378*, 2023.

Tim Salimans and Jonathan Ho. Progressive distillation for fast sampling of diffusion models. *arXiv:2202.00512*, 2022a.

Tero Karras, Miika Aittala, Jaakko Lehtinen, Janne Hellsten, Timo Aila, and Samuli Laine. Analyzing and Improving the Training Dynamics of Diffusion Models. *arXiv:2312.02696*, March 2024.

Cheng Lu and Yang Song. Simplifying, Stabilizing and Scaling Continuous-Time Consistency Models. *arXiv:2410.11081*, October 2024.

Tim Salimans and Jonathan Ho. Progressive Distillation for Fast Sampling of Diffusion Models. *arXiv:2202.00512*, 2022b.

Hongkai Zheng, Weili Nie, Arash Vahdat, Kamyar Azizzadenesheli, and Anima Anandkumar. Fast Sampling of Diffusion Models via Operator Learning. *arXiv:2211.13449*, 2023.

Tero Karras, Miika Aittala, Timo Aila, and Samuli Laine. Elucidating the Design Space of Diffusion-Based Generative Models. *arXiv:2206.00364*, 2022b.

## A Background on stochastic interpolants

For the reader’s convenience, we now recall how to construct probability flow equations using either flow matching with stochastic interpolants or score-based diffusion models. We also recall the connection between these two formalisms.

### A.1 Transport equation

The stochastic interpolant framework (1) gives a flexible and versatile way to build probability flows for generative modeling. Such generative models leverage the property that solutions to (2) push forward their initial conditions onto samples from the target, as we now show.

**Lemma A.1** (Transport equation). *Let  $\rho_t = \text{Law}(I_t)$  be the density of the solution to (2), assuming that  $x_0 \sim \rho_0$ . Then  $\rho_t$  satisfies the transport equation*

$$\partial_t \rho_t(x) + \nabla \cdot (b_t(x) \rho_t(x)) = 0, \quad \rho_{t=0}(x) = \rho_0(x) \quad (24)$$

where  $\nabla$  denotes a gradient with respect to  $x$ .

The above result implies that we can sample from any density  $\rho_t$  solving a transport equation of the form (24) by solving the corresponding ordinary differential equation (2).

*Proof.* The proof proceeds via the weak form of (24). Let  $\phi \in C_b^1(\mathbb{R}^d)$  denote an arbitrary test function. By definition,

$$\forall t \in [0, 1] \quad : \quad \int_{\mathbb{R}^d} \phi(x) \rho_t(x) dx = \mathbb{E}[\phi(I_t)] \quad (25)$$

where  $I_t$  is given by (1). Taking the time derivative of this equality, we deduce that

$$\begin{aligned} \int_{\mathbb{R}^d} \phi(x) \partial_t \rho_t(x) dx &= \mathbb{E}[\dot{I}_t \cdot \nabla \phi(I_t)] \\ &= \mathbb{E}[b_t(I_t) \cdot \nabla \phi(I_t)] \\ &= \int_{\mathbb{R}^d} b_t(x) \cdot \nabla \phi(x) \rho_t(x) dx. \end{aligned} \quad (26)$$

The first line follows by the chain rule, the second by the tower property of the conditional expectation and the definition of the drift  $b_t$ , and the third by definition of  $\rho_t$ . The last line is the weak form of the transport equation (24).  $\square$

## B Background on flow map matching.

As discussed in [Boffi et al. \(2024\)](#), given a pre-trained velocity field  $\hat{b}$ , we may leverage the three properties in Proposition 2.2 to design efficient distillation schemes by minimizing the corresponding square residual. To do so, rather than leveraging a single model of the form  $\hat{X}_{s,t}(x) = x + (t - s)\hat{v}_{s,t}(x)$  with  $\hat{v}$  serving as the self-teacher, we assume access to a pre-trained teacher velocity field  $\hat{b}$  or pre-trained teacher flow map  $\tilde{X}$ . In the following, we use the notation  $\mathcal{L}(\hat{X}; \hat{b})$  or  $\mathcal{L}(\hat{X}; \tilde{X})$  to denote a loss function for the flow map  $\hat{X}$  given the teacher (which remains frozen during training).

The first approach is the Lagrangian map distillation (LMD) algorithm, which is based on (8) and is the basis for the LSD algorithm,

$$\mathcal{L}_{\text{LMD}}(\hat{X}; \hat{b}) = \int_0^1 \int_0^t \mathbb{E}_{\rho_s} \left[ |\partial_t \hat{X}_{s,t}(I_s) - \hat{b}_t(\hat{X}_{s,t}(I_s))|^2 \right] ds dt. \quad (27)$$

A second scheme is the Eulerian map distillation (EMD) method based on (9). This approach recovers consistency distillation in the continuous-time limit ([Song and Dhariwal, 2023](#); [Lu and Song, 2024](#)), and is the starting point for consistency trajectory models ([Kim et al., 2024](#)).

$$\mathcal{L}_{\text{EMD}}(\hat{X}; \hat{b}) = \int_0^1 \int_0^t \mathbb{E}_{\rho_s} \left[ |\partial_s \hat{X}_{s,t}(I_s) + \nabla \hat{X}_{s,t}(I_s) \hat{b}_s(I_s)|^2 \right] ds dt. \quad (28)$$

Letting  $\tilde{X}_{\tau_1, \tau_2}$  denote either a pre-trained teacher flow map or the result of integrating the pre-trained probability flow  $\hat{b}$  over  $[\tau_1, \tau_2]$ , a final approach is progressive flow map matching (PFMM),

$$\mathcal{L}_{\text{PFMM}}(\hat{X}; \tilde{X}) = \int_0^1 \int_0^t \int_s^t \mathbb{E}_{\rho_s} \left[ |\hat{X}_{s,t}(I_s) - \tilde{X}_{u,t}(\tilde{X}_{s,u}(I_s))|^2 \right] du ds dt, \quad (29)$$

which is based on the semigroup property (10) and reduces to progressive distillation ([Salimans and Ho, 2022b](#)) and operator learning ([Zheng et al., 2023](#)). In words, (29) teaches  $\hat{X}$  to replicate two jumps of  $\tilde{X}$  in one larger jump. Our general self-distillation framework described in Section 2.3 may be obtained by using one of the above distillation schemes in tandem with direct training of  $\hat{v}$ , and where we use  $\hat{v}$  as the teacher velocity field for the student flow map model  $\hat{X}$ .

## C Proofs

In the following, we assume that all differential equations satisfy the following assumption.

**Assumption C.1.** *The drift satisfies the one-sided Lipschitz condition*

$$\exists C > 0 : \quad (b_t(x) - b_t(y)) \cdot (x - y) \leq C|x - y|^2 \quad \text{for all } (t, x, y) \in [0, 1] \times \mathbb{R}^d \times \mathbb{R}^d. \quad (30)$$

Under Assumption C.1, the classical Cauchy-Lipschitz theory guarantees that solutions exist and are unique for all  $x_0 \in \mathbb{R}^d$  and for all  $t \in [0, 1]$ .

We first provide a simple proof of the tangent condition we leverage in the main text.

**Lemma 2.1** (Tangent condition). *Let  $X_{s,t}$  denote the flow map. Then,*

$$\lim_{s \rightarrow t} \partial_t X_{s,t}(x) = b_t(x) \quad \forall t \in [0, 1], \quad \forall x \in \mathbb{R}^d, \quad (5)$$

*i.e. the tangent vectors to the curve  $(X_{s,t}(x))_{t \in [s, 1]}$  give the velocity field  $b_t(x)$  for every  $x$ .*

*Proof.* By Proposition 2.2, we have that the flow map satisfies the Lagrangian equation (8). Taking the limit as  $s \rightarrow t$ , we find

$$\lim_{s \rightarrow t} \partial_t X_{s,t}(x) = \lim_{s \rightarrow t} b_t(X_{s,t}(x)) = b_t(X_{t,t}(x)) = b_t(x). \quad (31)$$

Above, we used that  $X_{t,t}(x) = x$  for all  $x \in \mathbb{R}^d$  and for all  $t \in [0, 1]$ .  $\square$

We now recall our main proposition.

**Proposition 2.3** (Self-distillation). *The flow map  $X_{s,t}$  defined in (4) is given for all  $0 \leq s \leq t \leq 1$  by  $X_{s,t}(x) = x + (t-s)v_{s,t}(x)$  where  $v_{s,t}(x)$  the unique minimizer over  $\hat{v}$  of*

$$\mathcal{L}_{\text{SD}}(\hat{v}) = \mathcal{L}_b(\hat{v}) + \mathcal{L}_{\text{D}}(\hat{v}), \quad (11)$$

where  $\mathcal{L}_b(\hat{v})$  is given by

$$\mathcal{L}_b(\hat{v}) = \int_0^1 \mathbb{E}_{x_0, x_1} [|\hat{v}_{t,t}(I_t) - \dot{I}_t|^2] dt, \quad (12)$$

and where  $\mathcal{L}_{\text{D}}(\hat{v})$  is any linear combination of the following three objectives.

(i) The Lagrangian self-distillation (LSD) objective, which leverages (8),

$$\mathcal{L}_{\text{D}}^{\text{LSD}}(\hat{v}) = \int_0^1 \int_0^t \mathbb{E}_{x_0, x_1} [|\partial_t \hat{X}_{s,t}(I_s) - \hat{v}_{t,t}(\hat{X}_{s,t}(I_s))|^2] ds dt; \quad (13)$$

(ii) The Eulerian self-distillation (ESD) objective, which leverages (9),

$$\mathcal{L}_{\text{D}}^{\text{ESD}}(\hat{v}) = \int_0^1 \int_0^t \mathbb{E}_{x_0, x_1} [|\partial_s \hat{X}_{s,t}(I_s) + \nabla \hat{X}_{s,t}(I_s) \hat{v}_{t,t}(I_s)|^2] ds dt; \quad (14)$$

(iii) The progressive self-distillation (PSD) objective, which leverages (10),

$$\mathcal{L}_{\text{D}}^{\text{PSD}}(\hat{v}) = \int_0^1 \int_0^t \int_s^t \mathbb{E}_{x_0, x_1} [|\hat{X}_{s,t}(I_s) - \hat{X}_{u,t}(\hat{X}_{s,u}(I_s))|^2] du ds dt. \quad (15)$$

Above,  $\hat{X}_{s,t}(x) = x + (t-s)\hat{v}_{s,t}(x)$  and  $\mathbb{E}_{x_0, x_1}$  denotes an expectation over the random draws of  $(x_0, x_1)$  in the interpolant defined in (1).

We also recall our theoretical error bounds for the LSD and ESD algorithms.

**Proposition 2.4** (Wasserstein bounds). *Let  $\hat{X}_{s,t}(x) = x + (t-s)\hat{v}_{s,t}(x)$  denote a candidate flow map satisfying  $\mathcal{L}_b(\hat{v}) + \mathcal{L}_{\text{D}}^{\text{LSD}}(\hat{v}) \leq \varepsilon$ , and let  $\hat{\rho}_1$  denote the corresponding pushforward  $\hat{\rho}_1 = \hat{X}_{0,1} \# \rho_0$ . Let  $\hat{L}$  denote the spatial Lipschitz constant of  $\hat{v}_{t,t}(\cdot)$ . Then,*

$$W_2^2(\hat{\rho}_1, \rho_1) \leq 4e^{1+2\hat{L}}\varepsilon. \quad (16)$$

Now assume that  $\mathcal{L}_b(\hat{v}) + \mathcal{L}_{\text{D}}^{\text{ESD}}(\hat{v}) \leq \varepsilon$ . Then,

$$W_2^2(\hat{\rho}_1, \rho_1) \leq 2e(1 + e^{2\hat{L}})\varepsilon. \quad (17)$$

For ease of reading, we split the proofs of Proposition 2.3 and Proposition 2.4 into several intermediate results. We begin with our guarantees for the LSD algorithm.

**Proposition C.2** (Lagrangian self-distillation). *Consider the Lagrangian self-distillation method,*

$$\mathcal{L}_{\text{SD}}(\hat{X}) = \mathcal{L}_b(\hat{v}) + \mathcal{L}_{\text{D}}^{\text{LSD}}(\hat{v}). \quad (32)$$

*Then the unique global minimizer of (32) over all maps  $\hat{X}_{s,t}$  satisfying  $X_{t,t}(x) = x$  for all  $(x, t) \in \mathbb{R}^d \times [0, 1]$  is the flow map (4). Moreover, let  $\hat{X}$  denote a candidate flow map satisfying  $\mathcal{L}_{\text{SD}}(\hat{X}) \leq \varepsilon$ , and let  $\hat{\rho}_1$  denote the corresponding pushforward  $\hat{\rho}_1 = \hat{X}_{0,1} \# \rho_0$ . Let  $\hat{L}$  denote the spatial Lipschitz constant of  $\hat{v}_{t,t}(\cdot)$ . Then,*

$$W_2^2(\hat{\rho}_1, \rho_1) \leq 4e^{1+2\hat{L}}\varepsilon. \quad (33)$$

*Proof.* We first prove the statement of the global minimizer. Observe that for any  $\hat{b}$  and any  $\hat{X}$ ,

$$\begin{aligned} \mathcal{L}_b(\hat{b}) &\geq \mathcal{L}_b(b), \\ \mathcal{L}_{\text{D}}^{\text{LSD}}(\hat{v}) &\geq 0. \end{aligned} \quad (34)$$

where  $b_t(x) = \mathbb{E}[\dot{I}_t | I_t = x]$  is the ideal flow. This follows because  $\mathcal{L}_b$  is convex in  $\hat{b}$  with unique global minimizer given by  $b$ , while  $\mathcal{L}_{\text{D}}^{\text{LSD}}$  is a square residual term on the Lagrangian relation (8). From this, we conclude

$$\mathcal{L}_{\text{SD}}(\hat{X}) = \mathcal{L}_b(\hat{v}) + \mathcal{L}_{\text{D}}^{\text{LSD}}(\hat{v}) \geq \mathcal{L}_b(b). \quad (35)$$

By construction, the ideal flow map satisfies the Lagrangian equation (8). This, along with Lemma 2.1 implies that

$$\begin{aligned} v_{t,t}(x) &= b_t(x) & \forall (x, t) \in \mathbb{R}^d \times [0, 1], \\ \partial_t X_{s,t}(x) &= v_{t,t}(X_{s,t}(x)) & \forall (x, s, t) \in \mathbb{R}^d \times [0, 1]^2. \end{aligned} \quad (36)$$

From (36), we see that

$$\mathcal{L}_{\text{SD}}(X) = \mathcal{L}_b(v) + \mathcal{L}_{\text{D}}^{\text{LSD}}(v) = \mathcal{L}_b(v) = \mathcal{L}_b(b), \quad (37)$$

so that  $X_{s,t}$  achieves the lower bound (35) and is therefore optimal. Moreover, any global minimizer must satisfy (36), and the unique solution of these equations is the flow map, so that the global minimizer is unique.

We now prove the Wasserstein bound. Observe that  $\mathcal{L}_{\text{SD}}(\hat{X}) \leq \varepsilon$  implies that both  $\mathcal{L}_b(\hat{v}) \leq \varepsilon$  and  $\mathcal{L}_{\text{D}}^{\text{LSD}}(\hat{v}) \leq \varepsilon$ . We first note that

$$\begin{aligned} \mathcal{L}_b(\hat{v}) &= \int_0^1 \mathbb{E}_{\rho_t} [|\hat{v}_{t,t}(I_t) - \dot{I}_t|^2] dt, \\ &= \int_0^1 \mathbb{E}_{\rho_t} [|\hat{v}_{t,t}(I_t) - b_t(I_t)|^2] dt + \int_0^1 \mathbb{E}_{\rho_t} [|\dot{I}_t|^2 - |b_t(I_t)|^2] dt. \end{aligned} \quad (38)$$

In (38), we used that  $b_t(x) = \mathbb{E}[\dot{I}_t | I_t = x]$  along with the tower property of the conditional expectation. It then follows that the  $L_2$  error from the target flow  $b$  is bounded by

$$\int_0^1 \mathbb{E}_{\rho_t} [|\hat{v}_{t,t}(I_t) - b_t(I_t)|^2] dt \leq \varepsilon - \int_0^1 \mathbb{E}_{\rho_t} [|\dot{I}_t|^2 - |b_t(I_t)|^2] dt. \quad (39)$$

We now observe that, again by the tower property of the conditional expectation,

$$\begin{aligned} \int_0^1 \mathbb{E}_{\rho_t} [|\dot{I}_t|^2 - |b_t(I_t)|^2] dt &= \int_0^1 \mathbb{E}_{\rho_t} \left[ \mathbb{E} [|\dot{I}_t|^2 - |b_t(I_t)|^2 \mid I_t] \right] dt, \\ &= \int_0^1 \mathbb{E}_{\rho_t} \left[ \mathbb{E} [|\dot{I}_t - b_t(I_t)|^2 \mid I_t] \right] dt, \\ &\geq 0. \end{aligned} \quad (40)$$

Equation (40) shows that the term subtracted in (39) is a conditional variance, and therefore is nonnegative. Combining the two, we find that

$$\int_0^1 \mathbb{E}_{\rho_t} [|\hat{v}_{t,t}(I_t) - b_t(I_t)|^2] \leq \varepsilon. \quad (41)$$

We now consider the learned probability flow

$$\dot{\hat{x}}_t^v = \hat{v}_{t,t}(\hat{x}_t^v), \quad \hat{x}_0 \sim \rho_0. \quad (42)$$

By Proposition 3 of Albergo and Vanden-Eijnden (2022), (41) implies that

$$\mathcal{W}_2^2(\rho_1, \hat{\rho}_1^v) \leq e^{1+2\hat{L}} \varepsilon. \quad (43)$$

where  $\hat{\rho}_1^v = \text{Law}(\hat{x}_1^v)$ . Now, by Proposition 3.7 of Boffi et al. (2024),  $\mathcal{L}_{\text{D}}^{\text{LSD}}(\hat{v}) \leq \varepsilon$  implies

$$\mathcal{W}_2^2(\hat{\rho}_1^v, \hat{\rho}_1) \leq e^{1+2\hat{L}} \varepsilon. \quad (44)$$

By the triangle inequality and Young's inequality, we then have

$$\begin{aligned} \mathcal{W}_2^2(\rho_1, \hat{\rho}_1) &\leq 2(\mathcal{W}_2^2(\rho_1, \hat{\rho}_1^v) + \mathcal{W}_2^2(\hat{\rho}_1^v, \hat{\rho}_1)), \\ &\leq 4e^{1+2\hat{L}} \varepsilon. \end{aligned} \quad (45)$$

This completes the proof.  $\square$

We now prove a similar guarantee for the ESD method.

**Proposition C.3** (Eulerian self-distillation). *Consider the Eulerian self-distillation method,*

$$\mathcal{L}_{\text{SD}}(\hat{v}) = \mathcal{L}_b(\hat{v}) + \mathcal{L}_{\text{D}}^{\text{ESD}}(\hat{v}). \quad (46)$$

*Then the unique global minimizer of (46) over all maps  $\hat{X}_{s,t}$  satisfying  $X_{t,t}(x) = x$  for all  $(x, t) \in \mathbb{R}^d \times [0, 1]$  is the flow map (4). Moreover, let  $\hat{X}$  denote a candidate flow map with the same properties as in Proposition C.2. Then,*

$$\mathcal{W}_2^2(\hat{\rho}_1, \rho_1) \leq 2e(1 + e^{2\hat{L}})\varepsilon. \quad (47)$$

*Proof.* The proof follows a very similar structure to Proposition C.2. We first observe that for any  $\hat{v}$ ,

$$\begin{aligned} \mathcal{L}_b(\hat{v}) &\geq \mathcal{L}_b(b), \\ \mathcal{L}_{\text{D}}^{\text{ESD}}(\hat{v}) &\geq 0. \end{aligned} \quad (48)$$

From above, we conclude

$$\mathcal{L}_{\text{SD}}(\hat{v}) = \mathcal{L}_b(\hat{v}) + \mathcal{L}_{\text{D}}^{\text{ESD}}(\hat{v}) \geq \mathcal{L}_b(b). \quad (49)$$

Moreover, by the Eulerian equation (9), and by Lemma 2.1

$$\begin{aligned} v_{t,t}(x) &= b_t(x) & \forall (x, t) \in \mathbb{R}^d \times [0, 1], \\ \partial_s X_{s,t}(x) &= -\nabla X_{s,t}(x)v_{s,s} & \forall (x, s, t) \in \mathbb{R}^d \times [0, 1]^2. \end{aligned} \quad (50)$$

From (51), it follows that the ideal flow map satisfies

$$\mathcal{L}_{\text{SD}}(v) = \mathcal{L}_v(\phi) + \mathcal{L}_{\text{D}}^{\text{ESD}}(v) = \mathcal{L}_b(v) = \mathcal{L}_b(b). \quad (51)$$

Equation (51) shows that  $X_{s,t}$  achieves the lower bound (49) and hence is optimal. Moreover, because any global minimizer must satisfy (50), and because the unique solution to these equations is the flow map, the minimizer is unique.

We now prove the Wasserstein bound. As in Proposition C.2, our assumption  $\mathcal{L}_{\text{SD}}(\hat{v}) \leq \varepsilon$  implies that both  $\mathcal{L}_b(\hat{v}) \leq \varepsilon$  and  $\mathcal{L}_{\text{D}}^{\text{ESD}}(\hat{v}) \leq \varepsilon$ . Defining the flow  $\hat{x}_t^v$  as in (42), we have a bound identical to (43) on  $\mathcal{W}_2^2(\rho_1, \hat{\rho}_1^v)$ . Now, leveraging Proposition 3.8 in (Boffi et al., 2024), we have that

$$\mathcal{W}_2^2(\hat{\rho}_1^v, \hat{\rho}_1) \leq e\varepsilon. \quad (52)$$

Again applying the triangle inequality and Young's inequality yields the relation

$$\begin{aligned} \mathcal{W}_2^2(\rho_1, \hat{\rho}_1) &\leq 2(\mathcal{W}_2^2(\hat{\rho}_1^v, \hat{\rho}_1) + \mathcal{W}_2^2(\rho_1, \hat{\rho}_1^v)), \\ &\leq 2e(1 + e^{2\hat{L}})\varepsilon. \end{aligned} \quad (53)$$

This completes the proof.  $\square$

Finally, we prove that the minimizer is unique for the PSD approach.

**Proposition C.4** (Progressive self-distillation). *Consider the PSD method,*

$$\mathcal{L}_{\text{SD}}(\hat{v}) = \mathcal{L}_b(\hat{v}) + \mathcal{L}_{\text{D}}^{\text{PSD}}(\hat{v}) \quad (54)$$

*Then, for any  $p_\gamma$  with full support on  $[0, 1]$ , the unique global minimizer of (11) over all maps  $\hat{X}_{s,t}$  satisfying  $\hat{X}_{t,t}(x) = x$  for all  $(x, t) \in \mathbb{R}^d \times [0, 1]$  is the flow map (4).*

*Proof.* The proof follows by reduction to the Lagrangian equation (8). First, we observe that

$$\mathcal{L}_{\text{SD}}(\hat{v}) = \mathcal{L}_b(\hat{v}) + \mathcal{L}_{\text{D}}^{\text{PSD}}(\hat{v}) \geq \mathcal{L}_b(b). \quad (55)$$

By the semigroup property (10), we have that the true flow map satisfies

$$\mathcal{L}_{\text{SD}}(v) = \mathcal{L}_b(v) + \mathcal{L}_{\text{D}}^{\text{PSD}}(v) = \mathcal{L}_b(v) = \mathcal{L}_b(b), \quad (56)$$

so that  $X$  is optimal. Now, let  $X^*$  be any map satisfying

$$\mathcal{L}_{\text{SD}}(X^*) = \mathcal{L}_b(b), \quad (57)$$



i.e., any global minimizer of the PSD objective. It then necessarily follows that

$$\begin{aligned}\mathcal{L}_b(v^*) &= \mathcal{L}_b(v), \\ \mathcal{L}_D^{\text{PSD}}(v^*) &= 0.\end{aligned}\tag{58}$$

From (58), we have the tangent and semigroup conditions,

$$\begin{aligned}\lim_{s \rightarrow t} \partial_t X_{s,t}^*(x) &= b_t(x), & \forall (x, t) \in \mathbb{R}^d \times [0, 1], \\ X_{s,t}^*(x) &= X_{u,t}^*(X_{s,u}^*(x)), & \forall (x, s, u, t) \in \mathbb{R}^d \times [0, 1]^3.\end{aligned}\tag{59}$$

We claim that (59), along with  $X_{t,t}(x) = x$  for all  $(x, t) \in \mathbb{R}^d \times [0, 1]$ , imply that  $X^* = X$ . To see this, define the notation  $\partial_t X_{t,t}(y) = \lim_{s \rightarrow t} \partial_t X_{s,t}(y)$ . Then, consider a Taylor expansion of the infinitesimal semigroup condition for  $(x, s, t) \in \mathbb{R}^d \times [0, 1]^2$  arbitrary,

$$\begin{aligned}X_{s,t+h}^*(x) &= X_{t,t+h}^*(X_{s,t}^*(x)), \\ &= X_{t,t}^*(X_{s,t}^*(x)) + h \partial_t X_{t,t}^*(X_{s,t}^*(x)) + o(h), \\ &= X_{s,t}^*(x) + h \partial_t X_{t,t}^*(X_{s,t}^*(x)) + o(h), \\ &= X_{s,t}^*(x) + h b_t(X_{s,t}^*(x)) + o(h).\end{aligned}\tag{60}$$

Re-arranging, we find that

$$\frac{X_{s,t+h}^*(x) - X_{s,t}^*(x)}{h} = b_t(X_{s,t}^*(x)) + o(1),\tag{61}$$

so that

$$\lim_{h \rightarrow 0} \frac{X_{s,t+h}^*(x) - X_{s,t}^*(x)}{h} = \partial_t X_{s,t}^*(x) = b_t(X_{s,t}^*(x)).\tag{62}$$

Equation (62) is precisely the Lagrangian equation, whose unique solution is the ideal flow map. This completes the proof.  $\square$

## D Further details on self-distillation

**Semigroup parameterization.** By definition, we have that

$$X_{s,t}(x) = x + (t - s)v_{s,t}(x).\tag{63}$$

We then also have that

$$\begin{aligned}X_{s,u}(x) &= x + (u - s)v_{s,u}(x), \\ X_{u,t}(X_{s,u}(x)) &= X_{s,u}(x) + (t - u)v_{u,t}(X_{s,u}(x)), \\ &= x + (u - s)v_{s,u}(x) + (t - u)v_{u,t}(X_{s,u}(x)).\end{aligned}\tag{64}$$

By the semigroup property (10), it follows that

$$X_{s,t}(x) = X_{u,t}(X_{s,u}(x))\tag{65}$$

from which we see that

$$x + (t - s)v_{s,t}(x) = x + (u - s)v_{s,u}(x) + (t - u)v_{u,t}(X_{s,u}(x)).\tag{66}$$

Re-arranging and eliminating, we find that

$$v_{s,t}(x) = \left( \frac{u - s}{t - s} \right) v_{s,u}(x) + \left( \frac{t - u}{t - s} \right) v_{u,t}(X_{s,u}(x)),\tag{67}$$

which provides a direct signal for  $v_{s,t}$ . Choosing  $u = \gamma s + (1 - \gamma)t$  for  $\gamma \in [0, 1]$  leads to the simple relations

$$\frac{u - s}{t - s} = 1 - \gamma, \quad \frac{t - u}{t - s} = \gamma,\tag{68}$$

which can be used to precondition the relation (67) as

$$v_{s,t}(x) = (1 - \gamma)v_{s,u}(x) + \gamma v_{u,t}(X_{s,u}(x)).\tag{69}$$

In the numerical experiments, we use (69) to define a training signal for  $\hat{v}$ .

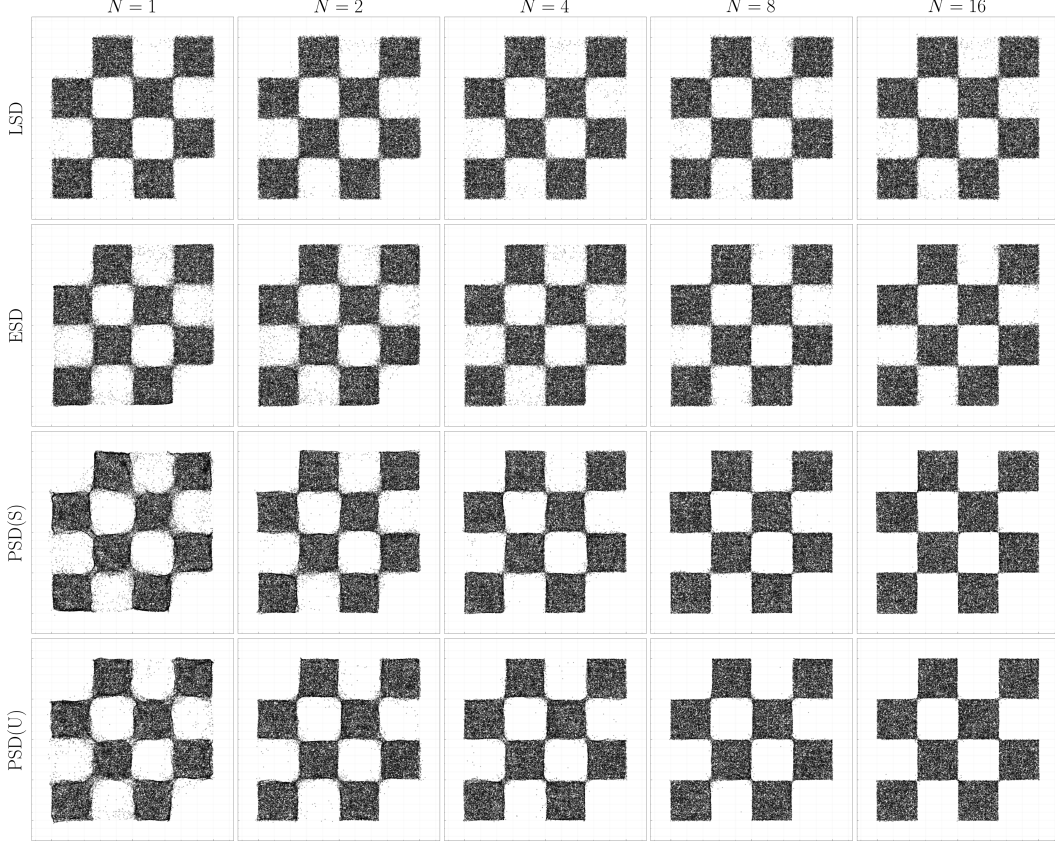


**Figure 6: (Checker: Full Results)** Full visualization of sample quality as a function of number of steps on the two-dimensional checker dataset.

**Limiting relations and annealing schemes.** As shown in the proof of Proposition 2.3, application of the semigroup property with  $(s, u, t) = (s, t, t + h)$  for a fixed  $(s, t)$  recovers the Lagrangian equation at order  $h$ . As shown in the proof of the tangent condition Lemma 2.1, the Lagrangian condition recovers the velocity field in the limit as  $s \rightarrow t$ . Similarly, if we consider the Eulerian equation in the limit as  $s \rightarrow t$ ,

$$\lim_{t \rightarrow s} \partial_s X_{s,t}(x) + \nabla X_{s,t}(x) b_s(x) = \partial_s X_{s,s}(x) + b_s(x) = 0, \quad (70)$$

so that  $\partial_s X_{s,s}(x) = -v_{s,s}(x) = -b_s(x)$ . In this way, all three characterizations reduce to the flow matching objective for  $v_{t,t}$  as the diagonal is approached. As a result, a natural annealing scheme is to follow an initial warmup phase based on pure flow matching for  $\hat{v}_{t,t}$  by progressively growing  $|t - s|$  to increase the range of step sizes.

## E Further details on numerical experiments

**Checker experiments.** We use a 4 hidden layer MLP architecture with 256 neurons per layer with the `gelu` activation function. We do not employ a learnable weighting  $w_{s,t}$ . We generate a dataset with  $10^7$  samples and train for 160,000 training steps with a batch size of 64,000 and a learning rate of  $10^{-3}$ . We employ the Adam optimizer. We use the linear interpolant with  $\alpha(t) = 1 - t$  and  $\beta(t) = t$  with a Gaussian base density,  $x_0 \sim N(0, I)$ . We leverage an annealing strategy in which we only train on the diagonal  $s = t$  for 5,000 steps, followed by a linear expansion of the range  $|t - s|$  for the next 5,000 steps. For the LSD and ESD algorithms, we do not employ a `sg` ( $\cdot$ ) operator in the loss function. For the PSD algorithms, we found improved performance by placing `sg` ( $\cdot$ ) on the teacher network. We use the instantaneous parameters for the teacher network rather than an EMA. We report results for the instantaneous parameters of the trained network and do not use an EMA. A

full qualitative visualization of the tabular results discussed in the main text is shown in Figure 6. Experiments were run on a single 40GB A100 GPU.

**CIFAR-10 Details** We use the EDM2 U-Net architecture with 128 channels, a channel multiplier of  $[2, 2, 2]$ , three blocks per residual layer, and attention at the  $8 \times 8$  and  $16 \times 16$  resolutions. We use positional embeddings, as we found that the usual Fourier embeddings caused even higher gradient variance with the LSD and ESD algorithms. We use dropout of 0.13, following the recommendations of EDM1 on CIFAR-10 (Karras et al., 2022b). We use 128 channels for the weight function  $w_{s,t}$ . We train with a batch size of 512 and a learning rate of  $10^{-3}$  with square root decay after 35,000 steps. We first train the velocity on the diagonal  $\hat{v}_{t,t}$  for 70,000 steps, followed by an annealing phase over  $|t - s|$  for 10,000 steps, followed by an additional 100,000 steps of training over the whole upper triangle. We use the Adam optimizer with the default settings. Experiments were run on 1-4 H100 GPUs, depending on availability. Several hyperparameter sweeps were used during initial experimentation and study phases before settling on these parameters.